Role of Pt in the Activity and Stability of PtNi/CeO2–Al2O3 Catalysts in Ethanol Steam Reforming for H2 Production

ARTICLE *in* TOPICS IN CATALYSIS · DECEMBER 2013

Impact Factor: 2.37 · DOI: 10.1007/s11244-013-0101-7

6 AUTHORS, INCLUDING:

Maricruz Sanchez-Sanchez
Technische Universität München
27 PUBLICATIONS **1,037** CITATIONS
SEE PROFILE

Adel Ismail
Central Metallurgical Research and Develo…
41 PUBLICATIONS **888** CITATIONS
SEE PROFILE

Top Catal (2013) 56:1672–1685
DOI 10.1007/s11244-013-0101-7

ORIGINAL PAPER

Role of Pt in the Activity and Stability of $PtNi/CeO_2–Al_2O_3$ Catalysts in Ethanol Steam Reforming for H_2 Production

M. C. Sanchez-Sanchez · R. M. Navarro · I. Espartero · A. A. Ismail · S. A. Al-Sayari · J. L. G. Fierro

Published online: 9 July 2013

Abstract Hydrogen production from ethanol reforming was investigated on bimetallic PtNi catalysts supported on CeO_2/Al_2O_3. Pt content was varied from 0.5 to 2.5 %. Physico-chemical characterization of the as-prepared and H_2-reduced catalysts by TPR, XRD and XPS showed that Pt phase interacted with the Ni and Ce species present at the surface of the catalysts. This interaction leads to an enhancement of the reducibility of both Ni and Ce species. Loadings of Pt higher than 1.0 wt% improved the activity and stability of the $Ni/CeO_2–Al_2O_3$ catalyst in ethanol steam reforming, in terms of lower formation of coke, C_2 secondary products and a constant production of CO_2 and H_2. The amount and type of carbon deposited on the catalyst was analyzed by TG–TPO while the changes in crystalline phases after reaction were studied by XRD. It was found that for Pt contents higher than 1 wt% in the catalysts, a better contact between Pt and Ce species is achieved. This Pt–Ce interaction facilitates the dispersion of small particles of Pt and thereby improves the reducibility of both Ce and Ni components at low temperatures. In this type of catalysts, the cooperative effect between Pt^0, Ni^0 and reduced Ce phases leads to an improvement in the stability of the catalysts: Ni provides activity in C–C bond breakage, Pt particles enhance the hydrogenation of coke precursors (C_xH_y) formed in the reaction, and Ce increases the availability of oxygen at the surface and thereby further enhances the gasification of carbon precursors.

Keywords Platinum catalyst activity for H_2 production · Ethanol · Steam reforming

M. C. Sanchez-Sanchez · R. M. Navarro · J. L. G. Fierro
Chemistry and Sustainable Energy Group, Instituto de Catalisis y Petroleoquimica (CSIC), C/Marie Curie s/n, Cantoblanco, 28049 Madrid, Spain
e-mail: jlgfierro@icp.csic.es

Present Address:
M. C. Sanchez-Sanchez (✉)
Catalysis Research Center, Technische Universität München, Lichtenbergstrasse 4, 85747 Garching, Germany
e-mail: maricruz.sanchez@tum.de

I. Espartero
Centro Nacional de Experimentación en Tecnologías del Hidrógeno y Pilas de Combustible, Puertollano, Ciudad Real, Spain

A. A. Ismail · S. A. Al-Sayari
Centre for Advanced Materials and Nanoengineering (CAMNE), Najran University, Najran 11001, Saudi Arabia

A. A. Ismail
Advanced Materials Department, Central Metallurgical R&D Institute, CMRDI, Helwan 11421, Egypt

1 Introduction

Hydrogen is considered to play a key role in the future energy systems as energy vector. Hydrogen is currently produced from non-renewable precursors (methane, hydrocarbons, etc.), which implies CO_2 as a byproduct in the transformation processes. In this context, there is an increasing interest in the development of technologies for the hydrogen production from biomass as a potential source of renewable energy. Among the chemicals derived from biomass, ethanol is of particular interest because: (i) it has low toxicity, (ii) it can be easily produced by fermentation of biomass such as sugar cane, waste materials from agro industries, or forestry residue, (iii) it is a relatively clean fuel in terms of composition, (iv) its hydrogen content is relatively high, and (v) as a liquid, it is easy to handle.

Ethanol can be efficiently converted in hydrogen by means of its catalytic reaction with steam according to the following reaction:

$$C_2H_5OH + 3\ H_2O \rightarrow 6\ H_2 + 2\ CO_2 \quad (1)$$

The ethanol steam reforming reaction includes several steps that involve the need for catalytic surfaces able to: (i) dehydrogenate ethanol, (ii) break the carbon–carbon bond of C_2 intermediates to produce CO and CH_4, and (iii) water reform the C_1 products to generate additional hydrogen. The requirements for the ethanol reforming catalysts are to present high yields of hydrogen and high selectivity to convert the carbon atoms in ethanol molecule into carbon oxides with minimum yields of residual hydrocarbons, as well as to be resistant to coke formation. Given the influence of the nature of both the metal and support on the catalytic characteristics of supported metals, a careful choice of these elements is a key factor to develop supported catalysts which fulfill the above requirements. The ethanol steam reforming reaction has been performed on several catalyst systems using Ni [1, 2], Co[3, 4], Ni/Cu [5, 6] and noble metals (Pd, Pt, Rh) [7–9] as active phases deposited on different oxide supports (e.g., Al_2O_3, La_2O_3, ZnO, MgO, etc.). Platinum group metals are, in general, more active for the steam reforming than non-noble transition metals, however they are more expensive. Although Ni catalysts are more prone to deactivation due to coke formation [10], they are preferred due to the lower cost of Ni. Coke formation is an important problem in ethanol reforming, and it appears to occur via a different mechanism in nickel than in noble metal-based catalysts. For nickel catalysts, filamentous carbon (whiskers) is formed at the surface of the metal particle by a consecutive process of formation, diffusion and dissolution. The platinum group metals have been reported to be more effective catalysts by preventing coke deposition since they do not dissolve carbon. Several authors have reported that the addition of small amounts of noble metals to Ni catalysts improved their catalytic performance [11–15]. Such improvement is mainly related to a lower formation of coke deposits on Ni surfaces. One explanation of this phenomenon is the role of noble metal in the hydrogenation of coke precursors adsorbed over the surface of the nickel particles [13, 16]. However, many questions related to the catalytic performance of Pt–Ni catalysts are still not answered to date.

The nature of support is the second element of catalyst formulation that strongly influences on the catalyst performance for the ethanol steam reforming reaction. Alumina-based supports are often used in steam reforming catalysts because of their chemical resistance under reaction conditions. However, the alumina surface acidity leads to an important production of ethylene, which can be easily dehydrogenated to form coke over Ni phases. Structural modifiers can be selectively added to Al_2O_3 in order to decrease the carbon formation associated with its acidity. For this purpose, rare earth elements are extensively used as promoters in the catalysts used in the reforming of ethanol [17, 18]. In particular, it is described in the literature that CeO_2 is able to store, release [19] and transport oxygen [20], and it adsorbs and activate steam [21]. For this reason, the presence of CeO_2 in Al_2O_3 support enhances the water gas shift reaction [22, 23], and promote the redox reversibility of the metallic phases [21]. Additionally, CeO_2 has been reported to prevent the loss of surface area of bare alumina [19, 24]. Likewise, it is well known the ability of CeO_2 to disperse Pt particles in its surface and inhibit their sinterization [19, 20, 25].

The present work aimed to investigate the role of Pt in modifying the textural, structural and surface properties of $Ni/CeO_2–Al_2O_3$ catalysts and how these properties influence on the catalytic behaviour for hydrogen production by steam reforming of ethanol. The Pt loading has been varied in order to study the role that this metal plays in the catalytic behavior, as well as to find an optimum amount that provides the desired promotion effect without increasing excessively the cost of the catalyst.

2 Experimental

2.1 Catalyst Preparation

$CeO_2–Al_2O_3$ support was prepared by impregnation of a commercial γ-Al_2O_3 (Alfa Aesar, S_{BET} 212 m^2/g) with an aqueous solution of $Ce(NO_3)_3$. The impregnated solid was dried under air at 393 K for 3 h and subsequently calcined at 923 K for 6 h.

Ni reference catalyst was prepared by impregnation of the $CeO_2–Al_2O_3$ support, with aqueous solutions of $Ni(NO_3)_2$. The catalyst (13 wt% Ni) was impregnated for 5 h, subsequently dried at 393 K for 2 h, and finally calcined in air at 773 K for 4 h.

Pt–Ni bimetallic catalysts were prepared by wet impregnation of the calcined $Ni/CeO_2–Al_2O_3$ catalyst with an aqueous solution of $Pt(NH_3)_4(NO_3)_2$ during 2 h. After drying at 383 K for 14 h, the Pt precursor was decomposed by treating the sample at 573 K under vacuum for 3 h. As a reference, a bimetallic catalyst was prepared by the same procedure but supported on bare Al_2O_3 calcined at 923 K.

Prior to the catalytic test, the catalysts must be activated in order to reduce the Ni particles. Therefore, the samples synthesized as described above (as-prepared samples) were treated under a flow of H_2 (10 vol%) for 1.5 h at 823 K (H_2-reduced samples).

2.2 Catalyst Characterization

The specific surface areas of the catalysts and support were calculated by applying the BET method to the N_2 adsorption isotherms, measured at liquid nitrogen temperature on a Micromeritics ASAP 2100 apparatus on samples previously degassed at 473 K for 24 h.

Temperature-programmed reduction experiments were carried out with a semiautomatic Micromeritics TPD/TPR 2900 apparatus equipped with a TC detector. Prior to reduction experiments, the samples, about 30 mg, were thermally treated under air stream at 573 K to remove water and other contaminants. TPR profiles were obtained by heating the samples under a 10 % H_2/Ar flow (50 mL/min) from 298 to 1,173 K at a linearly programmed rate of 10 K/min.

X-ray diffraction (XRD) patterns were recorded on reduced catalysts using a Seifert 3000P vertical diffractometer and nickel filtered Cu K_α radiation ($\lambda = 0.1538$ nm) under constant instrument parameters. For each sample Bragg angles between 5° and 80° were scanned. A rate of 5 s per step (step size: 0.04°2θ) was used during a continuous scan in the above mentioned range. Volume averaged crystallite sizes were determined by applying the Debye–Scherrer equation.

X-ray photoelectron spectroscopy (XPS) was used to study the chemical composition of the catalyst surfaces. Photoelectron spectra were recorded with a VG Escalab 200R electron spectrometer equipped with a Mg Kα X-ray source ($h\nu = 1{,}253.6$ eV) and a hemispherical electron analyzer operating at constant transmission energy (20 eV). The reduction treatment was carried out ex situ at 823 K in H_2/N_2 (1/9 vol) flow for 90 min followed by re-reduction in situ at 773 K for 30 min. The C 1 s, Al 2p, Pt 4d, Ce 3d and Ni 2p core-level spectra were recorded and the corresponding binding energies were referenced to the C 1 s line at 284.6 eV (accuracy within 0.1 eV).

Temperature programmed oxidation analyses of spent catalysts were carried out using a thermo-gravimetric analyzer (Mettler Toledo TGA/SDTA 851e) to determine the amount of coke deposited on catalysts. The standard protocol involved the weight change of the sample (20 mg) during its heating in 200 mL/min of N_2 as purge gas and 50 mL/min of O_2 as reactive gas from 298 to 1,373 K at a heating rate of 5 K/min.

2.3 Activity Tests

Activity tests were performed using 0.1 g of catalyst in the 0.4–0.5 mm particle size range (selected after preliminary mass transport experiments to minimize diffusional resistances) at a volume ratio of 3:1 to avoid adverse thermal effects. The catalyst bed was placed in a 6 mm ID quartz tubular reactor with a coaxially centred thermocouple. Prior to reaction, the catalysts were flushed in nitrogen at 473 K, followed by reduction in situ at 823 K for 1.5 h (heating rate 5 K/min) with 50 $mL_{(STP)}$/min of a 10 vol% H_2/N_2 mixture. Ethanol and water were feed independently into the pre-heater by means of syringe pumps (Becton–Dickinson) before mixing with carrier N_2. The samples were tested in steam reforming of ethanol (H_2O/EtOH(mol/mol) = 3.0, N_2 = 44 vol%) under a GHSV = 24,500 h^{-1} at atmospheric pressure and 773 K maintaining the reaction for 24 h in order to study the deactivation of the catalysts. The reaction products were analysed on-line by GC with TCD (Varian chromatograph Model Star 3400 CX) equipped with Porapack Q (CO_2, C_2H_6, C_2H_4, water, acetaldehyde, ethanol, acetone, acetic acid, diethyl ether, ethyl acetate, and crotonaldehyde) and molecular sieve 5A (H_2, O_2, N_2, CO) packed columns connected in series, using He as carrier gas.

3 Results

3.1 Chemical Composition and Textural Properties

Table 1 summarizes the chemical composition, expressed as weight percentages, and the textural properties measured by N_2 adsorption isotherms for the as-prepared catalysts and supports. For the sake of a valid comparison, the N_2 adsorption–desorption data were normalized to unit weight of Al_2O_3 support. As observed in Table 1, the addition of a 10 wt% of CeO_2 to Al_2O_3 support causes a slight decrease in its surface area and an increase in the pore diameter. Both facts are indicative of the partial blockage of the original pores of the Al_2O_3 by ceria species. The subsequent impregnation of the ACe support with nickel did not cause significant changes in its textural properties. Therefore the incorporation of Ni species on ACe support does not significantly alter the catalysts accessibility with respect to unloaded alumina support. On the contrary, the incorporation of Pt to NiACe slightly increased the surface area per gram of Al_2O_3 respect to that observed on NiACe before Pt impregnation. This fact might be indicative of dissolution/deposition of Ni and/or support particles during the Pt impregnation procedure.

3.2 Temperature-Programmed Reduction

In the Fig. 1, it is summarized the hydrogen consumption profiles during the temperature-programmed reduction experiments for the PtxNiACe samples and the NiACe reference catalyst.

For all the samples, a broad reduction peak is observed in the region 550–1,150 K, which can be decomposed into

Table 1 Chemical composition and textural properties of calcined supports and catalysts (N_2 adsorption–desorption isotherms at 77 K)

Sample	Pt wt. (%)	Ni wt. (%)	Ce wt. (%)	S_{BET} (m^2/g Al_2O_3)	V_{pore} (cm^3/g Al_2O_3)	D_{pore} (nm)
γ-Al_2O_3	–	–	–	235	0.82	13.9
ACe	–	–	9.9	212	0.81	15.2
NiACe	–	12.8	8.6	209	0.71	13.5
Pt05NiACe	0.5	12.7	8.6	222	0.75	13.7
Pt10NiACe	1.0	12.7	8.5	230	0.74	13.1
Pt25NiACe	2.5	12.5	8.4	250	0.83	13.3
Pt25NiA	2.5	12.6	–	225	0.85	15.0

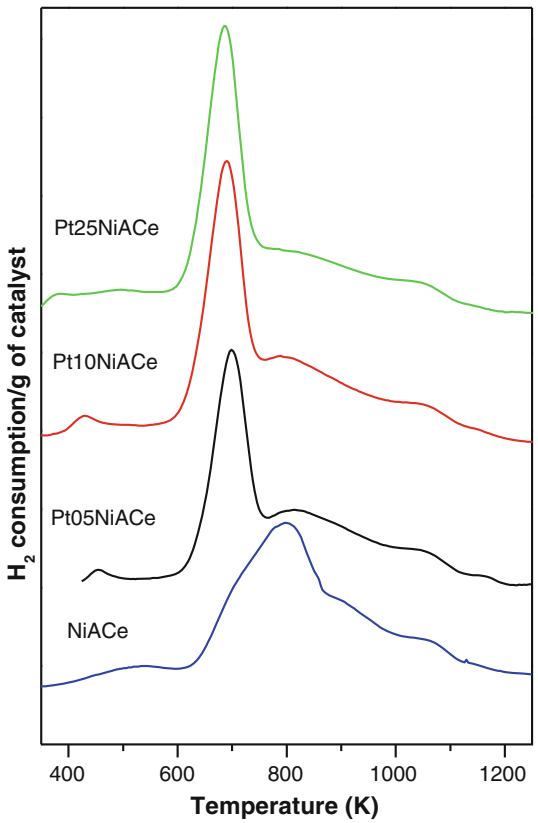

Fig. 1 Temperature-programmed reduction profiles of PtXNiACe and NiACe catalysts

several components. The NiACe catalyst showed three components, centered at 540, 800, 910 and 1,050 K, that can be assigned to the typical reduction of Ni^{2+} species formed in a Ni/Al_2O_3 catalyst prepared in similar conditions [26]. Such species are: (i) NiO species with weak interaction with alumina (reduction at 800 K); (ii) Ni^{2+} species in a non-stoichiometric nickel aluminate, also designated as amorphous surface spinel $NiAl_xO_y$ (hydrogen consumption at 910 K), and (iii) stoichiometric nickel aluminate $NiAl_2O_4$ species (typically reduced at 1,050 K) [27–29]. Apart from these Ni^{2+} species, the NiAlCe catalyst showed additional hydrogen consumption peak at 540 K, that could be ascribed to the reduction of NiO deposited on CeO_2 species [30], a shoulder centered at ca. 700 K, which is ascribed to the methanation of carbonate species formed on the CeO_2 species [31–33] and, finally, a very weak shoulder at high temperature (1,162 K), that is attributed to reduction of Ce^{4+} species strongly interacting with the alumina to form $CeAlO_3$ [34].

Strong changes were observed in the TPR profiles of the PtxNiACe catalysts respect to the NiACe counterpart even in the sample with the smallest Pt loading (Fig. 1). For the PtxNiACe samples, the most intense H_2 consumption peak is centered at 686–698 K. The relative intensity of this reduction peak increases and the maximum is shifted to lower temperatures with the Pt loading. The quantitative analysis of the H_2 consumption registered in the TPR experiments (not shown here) indicates H_2 consumption of this peak includes both the reduction of Ni^{2+} species, in NiO particles with weak interaction with the support, and some methanation of carbonate species formed on the CeO_2 surface as mentioned above. It is remarkable that the reduction of this type of Ni^{2+} species was recorded at temperatures ca. 120 K lower than in the NiAlCe reference catalyst. This phenomenon is attributed to a promoting effect of Pt on the reducibility of Ni species, in good agreement with the literature [35]. At higher temperatures, the TPR profile of PtxNiACe catalysts showed broad hydrogen consumption in the region 743–973 K that might include contributions of NiO particles with different degrees of interaction with the Al_2O_3, as well as surface $NiAl_xO_y$. The relative amount of these species decreased with the loading of Pt, due to an increase in the proportion of Ni species that can be already reduced at ca. 673 K. It is also observed that the maximum of this second main contribution is shifted to lower temperatures when increasing the loading of Pt, indicating again an enhancement of the reducibility of Ni by Pt phase. Finally, the hydrogen consumption centered at ca. 1,050 K appeared unchanged in all the catalysts, indicating that the presence of Pt on the surface did not affect the reducibility of bulk $NiAl_2O_4$.

The TPR profile of PtxNiACe catalysts showed, in addition, a reduction peak at $T < 523$ K, which is shifted to lower temperatures when the Pt loading increases. According to the literature [36, 37], H_2 consumption in this temperature interval might comprises both reduction of PtO_x over Al_2O_3 and partial reduction of surface ceria, promoted by Pt. Consistently, Pt loadings above 0.5 % shifted this peak to lower temperatures but did not increase its intensity, in good agreement with the literature about Pt–Ce–Al systems [36]. These results point to the existence of strong Pt–Ce interactions and are in good agreement

with the reported affinity of platinum for ceria phases when this metal is supported over CeO_2–Al_2O_3 systems [38].

From the results obtained in the TPR analyses of PtxNiACe samples, the activation temperature of catalysts was set at 823 K in order to reduce an important proportion of the Ni^{2+} species with weak and medium interaction with the support and to prevent the sinterization of Pt and/or Ni metal particles.

3.3 X-Ray Diffraction (XRD)

In the Fig. 2, the XRD patterns of as-prepared catalysts are shown. All samples present diffraction peaks at 2θ angles of 37.4, 46.0 and 68.8, characteristic of poorly crystalline γ-Al_2O_3 (JCPD 29-063). In addition, the as-prepared catalysts samples show well defined reflections at 2θ angles of 28.6, 33.1, 47.5, 56.3, 59.2, 76.6 and 79.1, attributed to bulk crystalline CeO_2 with fluorite structure (JCPD 34-394). The appearance of crystalline ceria structures indicates the saturation of the capacity of the Al_2O_3 support to disperse this species, which is in line with the dispersion limit for a CeO_2 monolayer on γ-Al_2O_3, established in 0.8 μmolCe/m^2 of Al_2O_3 by Damyanova et al. [39]. XRD patterns of the as-prepared bimetallic catalysts and the NiACe reference showed reflections at 43.3 and 62.9 characteristic of NiO crystalline phase (JCPD 78-643). The presence of $NiAl_2O_4$ would be difficult to determine by this technique, since the diffraction lines of this spinel phase are coincident with those or the γ-Al_2O_3 (pseudospinel phase). However, it is well known that materials with a high content in $NiAl_2O_4$ show a higher intensity of the diffraction line centered at 46.8° with respect to the line at 66.7° [27]. Therefore, one can conclude that the catalysts prepared in this study did not contain crystalline $NiAl_2O_4$. No diffraction peaks related to Pt phases were detected for any of the PtxNiACe, not even for the sample with the highest loading (2.5 wt%). This is due to the low concentration of Pt in the sample but it could also be a sign of the high dispersion of Pt species, since no periodic structures higher than 4 nm are observed. It is interesting to note that a similar catalyst of Pt (2.5 wt%) supported on Ni/Al_2O_3 without Ce, Pt25NiA, did show diffraction lines (not shown here) corresponding to Pt^0 crystallites of about 16 nm. This result points to the existence of strong Pt–Ce interactions, and is in good agreement with the reported affinity of platinum for ceria phases that enhances the dispersion of Pt on their surfaces.

The crystalline structure of the reduced catalysts has been also analyzed by XRD and the diffraction patterns are displayed in Fig. 3. The XRD profiles of reduced catalysts present reflections corresponding to CeO_2 and γ-Al_2O_3 phases. The relative intensity of CeO_2 diffraction lines with respect to alumina seems to have decreased after reduction treatment, indicating a lower amount of CeO_2 species in the reduced catalysts. In addition to γ-Al_2O_3 and CeO_2 phases, the diffraction patterns of the reduced catalysts showed lines at 2θ angles of 44.4, 51.8 and 76.3, attributed to metallic Ni phase (JCPD 04-850). On the other hand, the NiO phase has completely disappeared indicating a total reduction of the nickel particles detected in the as-prepared catalysts XRD patterns. For the PtxNiACe catalysts, very weak diffraction lines can be seen at 2θ angles 46.3° and ca. 39°, more intense in the sample with lower Pt content, indicating that some small amount of Pt^0 particles with particle size >4 nm might have been formed during the activation treatment. This results contrast with the XRD data obtained for the Pt25NiA reference (not shown here), where the 16 nm Pt^0 particles detected for the as-prepared catalyst sinterized to an average size of 20 nm after reduction.

The particle size of the Ni and Ce crystalline phases evaluated by XRD has been calculated for the catalysts before and after reduction (Table 2). The values (Table 2) were estimated by application of Scherrer' equation to the most intense diffraction peak of each phase involved (2 theta 43.3 for NiO, 44.5 for Ni^0 and at 28.6 for CeO_2). A careful deconvolution of the range 2 theta 40°–50° was done in order to subtract the contribution of diffraction peaks of alumina support to the Ni^0 and NiO features. In Table 2, it can be observed that NiO particles formed on CeO_2–Al_2O_3 support are in the range of 5–7 nm. It is observed a slight decrease of NiO particle size when the Pt loading increases. After reduction, the metallic Ni particles are ca. 1–2 nm smaller than the original NiO particles for all the catalysts except for the reference catalyst without Ce (Pt25NiA). Thus, it seems that the presence of CeO_2 on catalysts prevents sintering not only of Pt but also of Ni

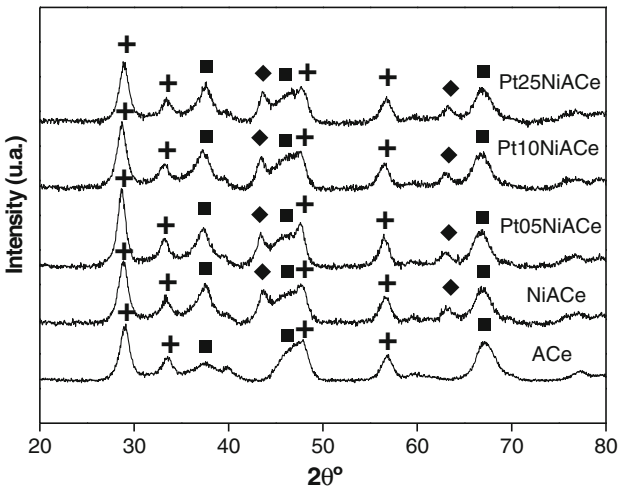

Fig. 2 XRD patterns of support and as-prepared catalysts (*filled square* Al_2O_3, *filled diamond* NiO, *plus* CeO_2)

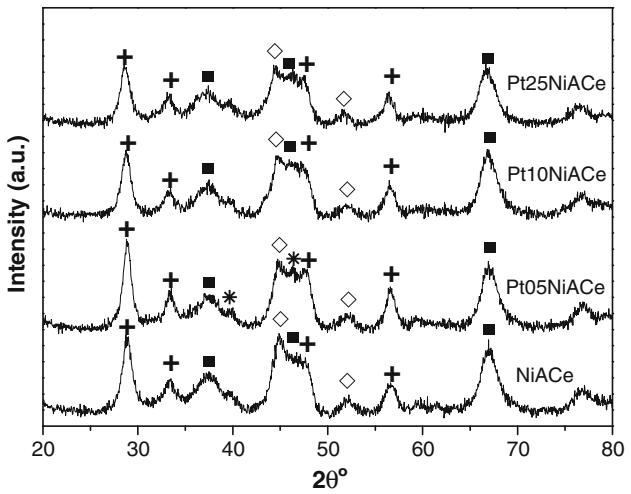

Fig. 3 XRD patterns of H_2-reduced catalysts (*filled square* Al_2O_3, *open diamond* Ni^0, *plus* CeO_2, *asterisks* Pt^0)

particles during the activation treatment. Regarding to Ce species, the size of the CeO_2 crystallites on the support remained almost unchanged after reduction, even though the intensity of the diffraction lines of CeO_2 fluorite have decreased with respect to Al_2O_3 diffraction line at 66°, which might indicate a partial reduction of CeO_2 to Ce^{3+} phases in quantities too small to be detected by this technique.

3.4 X-Ray Photoelectron Spectroscopy (XPS)

The binding energies of core-electrons Pt 4d, Al 2p, Ni 2p, Ce 3d, O 1 s and C 1 s have been recorded for the as-prepared catalysts by XPS and the results are summarized in Table 3. For platinum, due to the strong overlapping between Al 2p and Pt 4f peaks, only the Pt $4d_{5/2}$ energy region was scanned. This level showed three contributions centered at 315.0, 316.7 and 318.3 eV. The component at lower BE is assigned to metallic Pt species [40, 41] while the contributions in the energy range of 316.5–318.5 eV are usually ascribed to Pt^{2+} species. The presence of this latter Pt species is likely due to dispersed PtO_x particles interacting with the support [42]. The XPS spectra of Ni 2p level showed for all the catalysts the characteristic profile of Ni^{2+} species. In all the samples, Ni $2p_{3/2}$ binding energy is shifted to higher values than those typical for NiO (854 eV). This could be a consequence of the strong interaction between Ni^{2+} species and the support in the present catalysts. As it has been observed for other Ni/Al_2O_3 catalysts, some Ni^{2+} can be assimilated by the alumina structure giving rise to $NiAl_xO_y$ spinel [43]. The Ni 2p level for $NiAl_2O_4$ compound is recorded in the literature as 856.9 eV [44], which is a value much closer to our experimental results. Therefore, an important contribution for the Ni 2p surface signal is due to this type of species. Finally, the Ce $3d_{5/2}$ level was detected at a BE of 883.0 eV, characteristic of CeO_2. The contribution of the isolated peak in the Ce 3d spectra at ca. 917 eV to the total Ce 3d area (not shown here) indicates a very low fraction of Ce^{3+} species on the support [45]. The surface atomic ratios of the as-prepared samples, calculated from the intensities of the XPS peak normalized by atomic sensitivity factors [46] are also summarized in Table 3. It is observed that Pt/Al surface atomic ratio increases linearly with the Pt loading, indicating that the Pt phase is homogeneously introduced in the Ni–Ce–Al system. On the contrary, Ni/Al and Ce/Al surface atomic ratios decreased with higher loadings of Pt, which can be related to a preferential deposition of Pt on Ni and Ce species. The Ni/Ce surface ratio decreased with the addition of a 0.5 % of Pt, but it is observed to increase slightly with the introduction of higher loadings of Pt. This fact might indicate that the Pt is preferentially deposited on Ce.

The chemical state and relative proportion of catalysts constituents after reduction were also determined by photoelectron spectroscopy. The Al 2p, O 1 s, Ni 2p, Ce 3d and Pt 4d core-level spectra were recorded and the respective binding energy values are summarized in Table 4. Figure 4 displays the Ni 2p spectra of all H_2-reduced catalysts. The most intense line (Ni $2p_{3/2}$) of the Ni 2p emissions shows a component at 852.7–853.0 eV which is characteristic of Ni^0 [38] and a second one placed somewhere above 856 eV. Such a high binding energy and the observation of a satellite line around 861.4 eV are proof of the presence of Ni^{2+} ions in an environment of oxide ions, very likely in a $NiAl_2O_4$ structure [44].

From the spectra collected in Fig. 4 it is clear that the intensity of the component of metallic nickel increases with increasing Pt-loading in the catalysts (see also Table 4). The O 1 s peak appeared symmetric with a binding energy of 531.2–531.3 eV. This relatively high value indicates that the O 1 s line comes basically from the alumina substrate. For all reduced samples the binding energy of Pt $4d_{5/2}$ level observed at around 314.7 eV which is a value characteristic of metallic Pt. No shift in the binding energy of Pt 4d levels was observed and, therefore charge effects derived from Pt-

Table 2 Average crystalline particle size calculated from XRD

Sample	CeO_2	NiO (only in as-prepared)	Ni^0 (only in H_2-reduced)	Pt^0
NiACe	7/7	7	5	–
Pt05NiACe	8/7	6	5	n.d./?
Pt10NiACe	7/7	6	4	n.d./?
Pt25NiACe	7/7	5	4	n.d./?
Pt25NiA	–	7	10	16/20

(As-prepared/reduced)

Table 3 Binding energies (eV) of core-levels and surface atomic ratios from XPS analysis of support and as-prepared NiACe and PtxNiACe catalysts

Catalyst	BE Pt 4d (eV)[a]			BE Ni 2p (eV)	BE Ce 3d (eV)	Pt/Al	Ni/Al	Ce/Al
ACe	–	–	–	–	883.1	–	–	0.028
NiACe	–	–	–	856.7	883.1	–	0.100	0.016
Pt05NiACe	315.0	316.8	318.2	856.4	883.2	0.0010	0.092	0.023
	(39)	(28)	(33)					
Pt10NiACe	315.0	316.7	318.3	856.5	883.0	0.0018	0.090	0.033
	(32)	(46)	(22)					
Pt25NiACe	315.0	316.8	318.3	856.6	883.0	0.0046	0.076	0.016
	(34)	(39)	(27)					

[a] In brackets, contribution to the total signal to the level Pt 4d, in percentage

Table 4 Binding energies (eV) of core-levels and surface atomic ratios from XPS analysis of H2-reduced NiACe reference and PtxNiACe catalysts

Catalyst	BE Al 2p	BE Ni $2p^{a}_{3/2}$	BE Ce $3d^{b}_{5/2}$	BE Pt $4d_{5/2}$	Ni/Al	Ce/Al	Pt/Al
NiACe	74.5	853.0 (14)	881.9	–	0.067	0.058	–
		856.5 (86)	(30.3)				
Pt05NiACe	74.5	852.7 (26)	882.3	314.7	0.063	0.039	0.0021
		856.3 (74)	(32.6)				
Pt10NiACe	74.5	852.6 (29)	882.1	314.8	0.070	0.041	0.0042
		856.3 (71)	(43.9)				
Pt25NiACe	74.5	852.8 (31)	882.1	314.7	0.090	0.049	0.0091
		856.5 (69)	(37.7)				

[a] In brackets, contribution to the total Ni 2p level signal in percentage

[b] In brackets, percentage of Ce^{3+} species, calculated by Eq. (2)

support or Pt–Ni interactions are not observed by this technique. Nevertheless the possibility of partial electronic interactions at interface level between Pt and Ni or support could not be discarded because the difficulty to detect these interactions by this technique.

The Ce 3d core level spectra of the H_2-reduced catalysts are displayed in Fig. 5. As it can be seen, both Ce^{3+} and Ce^{4+} oxides are present and their signals appear crowded within a binding energy interval of ca. 35 eV [47]. The proportion of Ce^{3+} in the reduced catalysts was also evaluated. The Ce^{3+} percentage was calculated by taking into account the Ce $3d_{3/2}$ line according to the following expression [48]:

$$\%\ Ce^{3+}_{(3/2)} = A\ Ce^{3+}_{(3/2)} / \left[A\ Ce^{3+}_{(3/2)} + A\ Ce^{4+}_{(3/2)}\right] \qquad (2)$$

where A Ce^{3+} and A Ce^{4+} denote the total intensity by area in the Ce $3d_{3/2}$ component relevant to the Ce^{3+} and Ce^{4+} ions, respectively [48]. The deconvolution of Ce 3d level is shown in Fig. 5. The percentages of $Ce^{3+}_{(3/2)}$ in reduced catalysts are also collected in Table 4. It appears that this percentage increases when Pt is incorporated and reaches a maximum for the Pt10NiACe catalyst. A similar calculation was done by applying Eq. (2) to the most intense $Ce^{3+}_{(5/2)}$ level. The percentage of reduced cerium was similar although deviation of results was within 9 %.

The surface atomic ratios, calculated from the intensities of the peak normalized by atomic sensitivity factors [45] are summarized in Table 4. Ce/Al ratios were in every case higher after reduction, indicating a partial covering of metal particles with Ce entities, as it was reported in the literature [49, 50]. The surface exposition of the Ce species increased linearly with Pt loading in the bimetallic catalysts. After reduction, it is observed that for catalysts with up to 1.0 wt% Pt loading the amount of Ni at the surface has decreased. This effect has been typically observed for Ni/Al_2O_3 catalysts [51], and it is explained by a 'decoration' of metallic particles by dispersed species from alumina support after reduction of surface $NiAl_xO_y$ layer covering the NiO particles [43, 52]. However, the XPS Ni/Al ratio calculated for reduced PtxNiACe catalysts increases slightly with Pt content, suggesting that Ni dispersion is favored by this species. In the case of the catalyst Pt25NiACe this dispersive effect of the Pt on the Ni phase is so strong that the Ni/Al XPS signal increased during the reduction treatment. The percentage of the Ni 2p core level XPS signal due to metallic Ni (Fig. 4) was also calculated

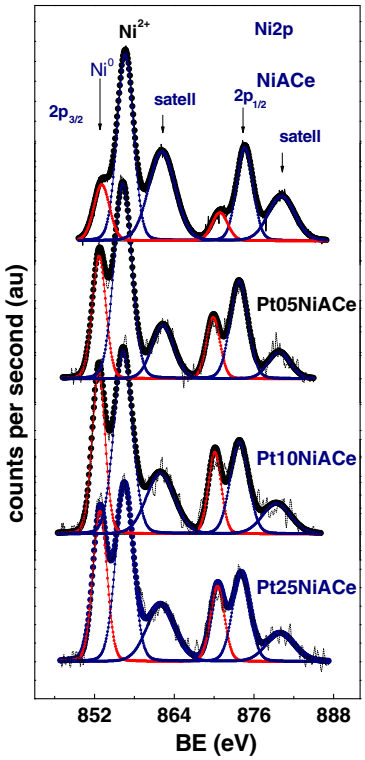

Fig. 4 XPS Ni 2p spectra of H_2-reduced catalysts

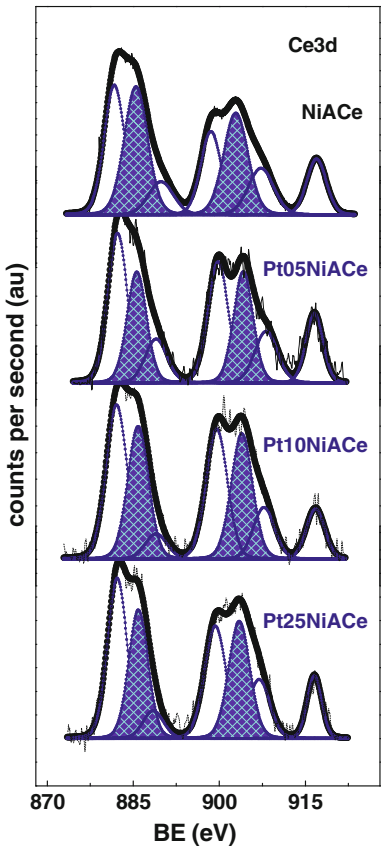

Fig. 5 XPS Ce 3d spectra of H_2-reduced catalysts

and it is summarized in the Table 4. It can be observed that the amount of metallic Ni at the surface slightly increases with Pt loading. A significant increment was achieved with only 0.5 % of Pt, in good agreement with TPR results, and additional reduction of Ni particles is observed by further increase of Pt loading. This, together with the calculated Ni/Al surface ratio, indicates that the overall surface concentration of Ni^0 species increases with the content of Pt in the sample. Finally, it is observed that Pt/Al and Pt/Ni surface ratios are higher than those calculated for the respective calcined catalysts prior reduction, indicating a high dispersion of Pt phases. Only Pt/Ce was observed to decrease after reduction for catalyst Pt25NiACe, probably due to the high Ce dispersion detected for this sample.

3.5 Catalytic Activity

The conversion of ethanol and the distribution of products for the steam reforming of ethanol over PtxNiACe catalysts and the reference catalyst NiACe are plotted in Fig. 6. The selectivity to products achieved at steady state (ca. 20 h on stream) is displayed in Table 5. In Fig. 6a, the results of the catalytic test for NiACe reference catalyst are summarized. It is observed that in the first hours in reaction, the NiACe catalyst converted ethanol totally into H_2, CO_2, CO and CH_4 products. This indicates that the catalyst is active in the dehydrogenation of ethanol and subsequent C–C bond scission of acetaldehyde to CH_4 and CO. However after ca. 4 h under reaction conditions, the selectivity toward products changed and C_2H_4, CO, CO_2 and H_2 were the only products after 24 h on-stream. The disappearance of CH_4 product is assigned to a partial deactivation of the metal phases, which have lost the ability to transform ethanol through the dehydrogenation pathway to acetaldehyde and subsequent decomposition to CO and CH_4 [16]. After this partial deactivation, a higher amount of ethanol is available to be dehydrated on the Al_2O_3 acid sites [53] to form ethylene, which eventually might access some of the Ni active particles and be reformed to CO_x and H_2. However, it should be noted that ethylene in presence of Ni particles has a high tendency to form coke deposits, and in particular carbon filaments [54].

The catalyst containing a 0.5 wt% of Pt showed a catalytic behavior similar to the one observed for NiACe reference catalyst (Fig. 6b). In this case, traces of ethane were also detected. As platinum is highly active in hydrogenation of alkenes, the formation of ethane is attributed to the hydrogenation of ethylene intermediate on Pt particles. Nevertheless, the hydrogenation activity of Pt particles seems to be inhibited after a few hours under reaction conditions. As can be seen in Table 5, the product distribution of the catalyst after 20 h reaction time is very similar to NiACe reference, with a H_2 selectivity higher for Pt05NiACe due to a slightly lower production of CH_4 and C_2H_4. This can be interpreted

as an overall lower deactivation degree of Pt05NiACe with respect to NiACe.

The Pt10NiACe and Pt25NiCe catalysts (Fig. 6c, d) were highly active and stable in transforming ethanol into the reforming products H_2 and CO_2 (only 10 % of products are CH_4 and CO). For this catalyst formulation it was not observed production of C_2H_4 or C_2H_6 during the 24 h of duration of the catalytic test. This indicates that the metal particles on catalysts with higher Pt loading, Pt10NiACe and Pt25NiACe samples, did not show a partial deactivation process as observed previously in the NiACe and Pt05NiACe counterparts. Longer activity tests would be necessary in order to determine if the introduction of a higher amount of Pt provides the catalyst with better stability.

3.6 Characterization of Used Catalysts

The XRD profiles recorded for the catalysts used for 24 h in ethanol steam reforming are displayed in Fig. 7. Diffraction lines for Ni^0 (JCPD 04-850), γ-Al_2O_3 (JCPD 29-063) and CeO_2 (JCPD 34-394) phases are observed. In addition, a broad diffraction peak centered at 2θ ca. 26° is detected for all the samples. This diffraction line is characteristic of graphitic carbon (JCPD 75-1621), and indicates that coke deposition took place during the ethanol steam reforming under the selected reaction conditions. Due to a dilution effect of the graphitic carbon, the quality of the diffraction peaks of the catalysts did not allow the deconvolution of the complex feature at 2θ 41°–50° and

Table 5 Selectivity toward products in percentage, obtained for NiACe reference and PtXNiACe catalysts in ethanol steam reforming (773 K, H_2O/EtOH = 3.0, N_2 = 44 vol%, GHSV = 24,500 h^{-1}, total ethanol conversion) after 20 h on stream

	H_2	CO_2	CH_4	CO	C_2H_x
NiACe	47.9	21.9	2.4	4.4	23.4
Pt05NiACe	49.4	21.4	1.5	4.8	22.9
Pt10NiACe	60.8	33.6	2.9	2.7	0.0
Pt25NiACe	60.7	28.9	7.3	3.1	0.0

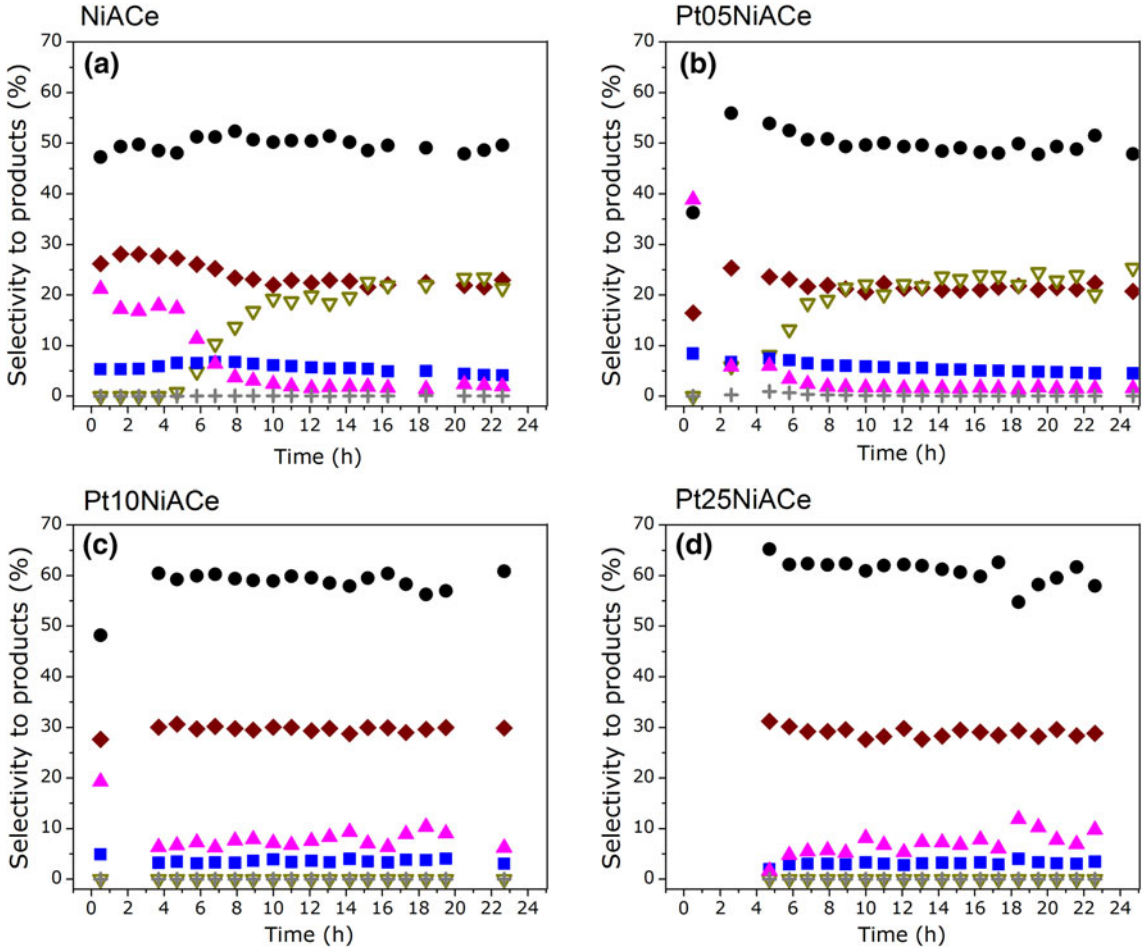

Fig. 6 Catalytic activity in ethanol steam reforming at 773 K, H_2O/EtOH(mol/mol) = 3.0, N_2 = 44 vol%, GHSV = 24,500 h^{-1} of samples **a** NiACe, **b** Pt05NiACe, **c** Pt10NiACe and **d** Pt25NiACe. Total ethanol conversion, selectivity to products *filled circle* H_2, *filled diamond* CO_2, *filled up-pointing triangle* CH_4, *filled square* CO, *open down-pointing triangle* C_2H_4, *plus* C_2H_6

therefore the particle size of the crystalline phases were not calculated. However we can analyze the evolution of the Ni^0 phases after reaction by comparing the relative intensity of the Ni diffraction line respect to alumina diffraction line at 66.5° which, in principle, should remain unchanged. Based on that observation, some sintering of the Ni^0 particles under reaction conditions can be expected.

Because of the intense contribution of the Ni^0 particles to this 2θ region, it is difficult to observe the features corresponding to Pt^0 phases. Only in the case of sample Pt25NiACe it can be observed that a peak has appeared at 2θ angles of ca. 43°, corresponding to NiO phase. Consistently, the intensity of Ni^0 diffraction line at 44.8° was lower and the diffraction line at 52° has almost disappeared, indicating some reoxidation of Ni species under reaction atmosphere.

Regarding to Ce species, it is observed that the diffraction lines of CeO_2 fluorite phase are more intense after reaction for the sample Pt05NiACe. On the contrary, for samples Pt10NiACe and Pt25NiACe the diffraction lines of CeO_2 phase are weaker after reaction if compared with the XRD diffractograms of reduced catalysts (Fig. 3), indicating a loss of crystallinity of Ce species.

Thermogravimetric analyses of the spent catalysts and supports were carried out to calculate the amount of carbonaceous residues retained in the catalysts after reaction by measuring the weight loss during its temperature-programmed oxidation under a 20 % O_2 gas flow. In the Fig. 8 are represented the TG–TPO profiles (as derivative of weight) of the catalysts used in ethanol steam reforming reaction. All the used catalysts showed a weight loss in the temperature range 573–873 K. The complex TG–TGO profile observed on all used samples, with multiple contributions, indicates that carbon deposits of different nature were formed on used catalysts. The contribution centered at 673–723 K is assigned to the gasification of carbonate species, formed on the surface of CeO_2, given the ability of this oxide to react with CO_2 [55]. The samples with low or no content in Pt are able to gasify this carbonate species only when temperature reaches ca. 728 K, while samples Pt10NiACe and Pt25NiACe showed this shoulder centered at ca. 708 and 688 K, respectively. The oxidation peak with a maximum centered at 750–790 K has been identified by several authors as the gasification of C_xH_y intermediates formed by dehydrogenation of methane and ethylene intermediates [56, 57]. The maximum of oxidation of these carbonaceous species is shifted to lower values with the loading of Pt (787 K for NiACe reference, 753 K for Pt25NiACe), indicating that the presence of Pt enhances the gasification of C_xH_y intermediates. Finally, the broad contribution observed at higher oxidation temperatures, with a maximum centered at 773–810 K is attributed to the gasification of coke deposits with some degree of graphitization. As with the gasification of C_xH_y intermediates, the presence of Pt shifted to lower temperatures the oxidation of this species (from ca. 811 K for NiACe to 795 K for Pt10NiACe). For the sample Pt25NiACe, the shift of the gasification temperature for graphitic carbon might be so that it takes place simultaneously to the gasification of

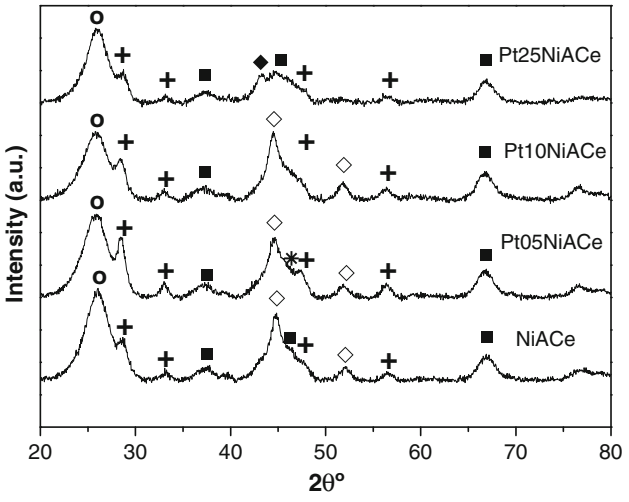

Fig. 7 X-ray diffractograms registered for the catalysts used for 24 h in ethanol steam reforming (773 K, H_2O/EtOH = 3.0, N_2 = 44 vol%, GHSV = 24,500 h^{-1}). *Filled square* Al_2O_3, *open diamond* Ni^0, *plus* CeO_2, *filled diamond* NiO, *open circle* graphite

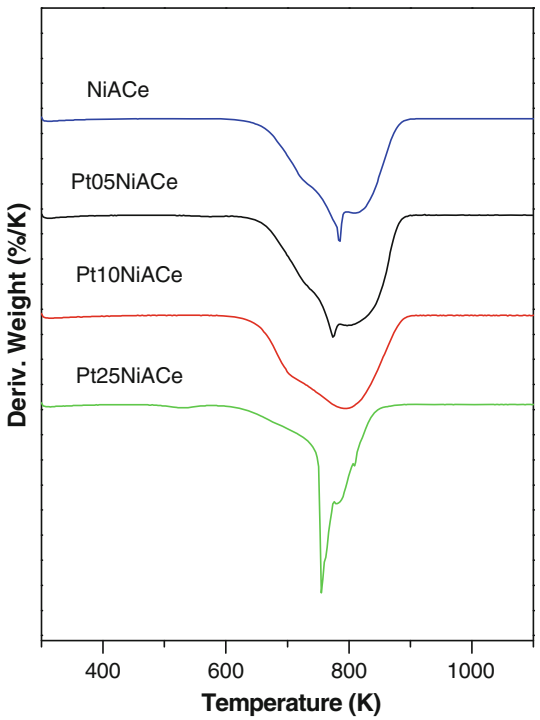

Fig. 8 TG–TPO profiles of used catalysts after 24 h in ethanol steam reforming (773 K, H_2O/EtOH = 3.0, N_2 = 44 vol%, GHSV = 24500 h^{-1})

C_xH_y, making it difficult to identify the two types of carbonaceous species.

Quantification of TG–TPO analyses was done and the results are summarized in Table 6. It is well known that Ni catalysts tend to form carbon filaments in reforming reactions [54]. In the literature, CeO_2 species have been reported to effectively gasify coke precursors by means of the formation of a carbonate intermediate [58, 59]. Therefore, the amount of carbon formed on the NiACe reference catalyst is relatively low in comparison to the carbon formation on a Ni/Al_2O_3 in the same reactions conditions [51]. In addition to the beneficial effect of Ce, the carbon formation per gram of catalyst is observed to decrease linearly with the Pt loading (Table 6).

4 Discussion

The characterization of ACe support by XRD and N_2 isotherm showed that Ce species formed CeO_2 crystallites on the surface of the alumina, producing some pore blockage (Table 1). However, the subsequent impregnation of the CeO_2/Al_2O_3 support with Ni and Pt did not cause significant changes in the textural properties, indicating that the new phase was adequately dispersed.

The analysis of the catalysts by XRD has shown that as-prepared samples contained NiO particles with an average size in the range of 5–7 nm. The absence of diffraction lines for Pt phases indicates that Pt particles should be <4 nm. It should be noted that the high dispersion of Pt phases is related to the ability of CeO_2 to disperse this metal, because bare γ-Al_2O_3 demonstrated to achieve low Pt dispersion at this loading (as can be seen for reference catalyst Pt25NiA in Table 2). Formation of nickel aluminate has been detected by XPS (Table 3) and by TPR (Fig. 1). By analysis of the data from TPR, it can be seen that two types of aluminates are formed: non-stoichiometric $NiAl_xO_y$ and stoichiometric $NiAl_2O_4$. The latter species is not affected by the loading of Pt, while non-stoichiometric aluminate was observed to interact with Pt species, as it is revealed by the shift of $NiAl_xO_y$ reduction temperature to lower values (Fig. 1). This, together with the important contribution of the Ni^{2+} species in an aluminate environment (BE > 856 eV) to the XPS Ni 2p level, verifies the surface character of this species. It should be noted that in spite of the strong effect of Pt on Ni and Ce reducibility, no shift in the binding energies of Pt 4d, Ni 2p or Ce 3d levels was observed by XPS. Therefore, charge effects derived from Pt-support or Pt–Ni interactions are not proven by this technique. Nevertheless the possibility of partial electronic interactions at interface level between Pt and Ni or support could not be discarded.

According to XRD analyses (Table 1), the Ni^0 particles formed after activation are smaller than the original NiO particles before activation. Additionally, the size of Ni^0 particles decreased with the addition of higher amounts of Pt. The addition of Pt to $Ni/CeO_2–Al_2O_3$ samples, as it was already mentioned, was observed to enhance the reducibility of Ni^{2+} species, including non-stoichiometric $NiAl_xO_y$ entities. This enhancement of Ni reducibility is attributed to the H_2 spillover on Pt particles [60], which produces a higher mobility of hydrogen on the support surface, facilitating the access to Ni particles. Given that the Pt loading shifts the reduction of all Ni species to lower temperatures (Fig. 1), it is expected that a higher amount of non-stoichiometric $NiAl_xO_y$ species can be reduced during the activation treatment for samples with higher content in Pt. As a consequence of the reduction of these $NiAl_xO_y$ species, very small Ni^0 particles are generated, decreasing the average particle size of this phase [26] and increasing, therefore, the surface proportion of metallic Ni (Table 4; Fig. 4). Even for low amounts of Pt (0.5 wt%) added to NiACe catalyst, a significant increment of the Ni^0 at the surface (calculated by XPS, Table 4) is achieved with respect to the reference NiACe, in good agreement with TPR results.

It should be mentioned that the CeO_2 species also played a role in the dispersion of metallic Ni and Pt phases obtained after reduction. According to Zheng et al. [61], the presence of Ce on alumina supports can hinder the sintering of Ni particles by inhibiting the surface mobility of Ni atoms. It can be observed in Table 2 that the reduction treatment caused the sintering of both Pt and Ni metal on a $PtNi/Al_2O_3$ catalyst without ceria loading. On the contrary, the samples containing ceria in the support show after reduction very weak diffraction lines at 2θ angles 46.3° and ca. 39° pointed to some small amount of Pt^0 particles with particle size >4 nm. Interestingly, the sample showing these lines better defined was Pt05NiACe, with only a 0.5 % of Pt. This might be indicative of a deficient Pt–Ce interaction for this catalyst, probably due to a lower amount of Ce species at the surface of this sample, as it will be explained below.

Table 6 Carbon deposits on used catalysts quantified by TG–TPO analysis after 24 h in ethanol steam reforming (773 K, H_2O/EtOH = 3.0, N_2 = 44 vol%, GHSV = 24,500 h^{-1})

Sample	g coke/g cat
NiACe	0.660
Pt05NiACe	0.644
Pt10NiACe	0.629
Pt25NiACe	0.583

The TPR profiles of bimetallic PtxNiACe catalysts showed that the reducibility of surface Ce species was also facilitated by the presence of Pt particles, even for small loadings of Pt, due to an activation of the H_2 molecules on this metal [62]. The reduction of highly dispersed Ce^{4+} species was confirmed by the XPS Ce 3d core level spectra recorded for the samples after reduction (Fig. 5). In Table 4, it can be seen that the percentage of Ce^{3+} species at the surface increases when Pt is incorporated and reaches a maximum for the Pt10NiACe catalyst. In agreement with observations from TPR and XPS techniques, the CeO_2 XRD diffraction lines were observed to decrease in intensity with respect to Al_2O_3 species in reduced catalysts, providing further evidence of a partial reduction of CeO_2 during the activation treatment applied. The reduction process of Ce^{4+} species seems to bring a higher dispersion of Ce on the surface (Table 4).

The selectivity toward products in the ethanol steam reforming on NiACe reference catalyst and Pt05NiACe catalyst changed with time on stream (Fig. 6a, b). Production of C_2H_4 increased at the expense of disappearance of CH_4 in the gas products. This change in product distribution is attributed to the partial deactivation of the metal phases, which turns into a low ability to transform ethanol through the dehydrogenation pathway to acetaldehyde and subsequent decomposition to CO and CH_4 [16]. The production of ethylene by ethanol dehydration on Al_2O_3 acid sites [53] is related to a higher formation of coke deposits (carbon filaments) [54]. This was confirmed by TG–TPO quantification of the carbon deposits, showing the highest values of g_{coke}/g_{cat} for NiACe and Pt05NiACe (Table 6). On the contrary, catalysts Pt10NiACe and Pt25NiACe did not produce any C_2 product during the 24 h of duration of the catalytic test (Fig. 6c, d). In other words, they did not suffer deactivation of the C–C cleavage functionality, as it was observed for catalysts with Pt loadings bellow 1.0 wt %. The Pt10NiACe catalyst achieved steady state after only 4 h and was able to convert ethanol to reforming products CO_2 and H_2 with a 90 % of selectivity (Table 5). The sample Pt25NiACe selectivity to reforming products was 96 % after 4 h on stream but it decreased later to a stable $H_2 + CO_2$ production of 90 %. In any case, longer activity tests would be necessary in order to determine if introduction of a higher amount of Pt provides the catalyst with an actual better stability.

As it is already mentioned, the quantification of the carbon deposits by TG–TPO showed that the coke formation decreased linearly with the Pt loading. This observation indicates that Pt species are involved in the gasification of coke precursors, which are probably formed on Ni particles [54]. It has been reported [16] that for PtNi bimetallic catalysts high stability in ethanol steam reforming is achieved by means of a cooperative effect of both Pt and Ni phases: Ni provides activity in C–C bond breakage and Pt particles enhance the mobility of the H_2 formed in the reaction, helping to gasify the carbon precursors.

In this study, it has been observed that a Pt loading $\geq$1.0 wt% is necessary to improve the stability of Ni/CeO_2–Al_2O_3 catalysts in the steam reforming of ethanol. For lower Pt loading (Pt05NiACe) it is also observed an improvement in the stability of the Ni/CeO_2–Al_2O_3 catalyst but in much less extent. In the characterization of the Pt05NiACe sample by TPR, it was detected the existence of a certain amount of Ce species with strong interaction with the Al_2O_3, forming $CeAlO_3$ precursor. Pt05NiACe also showed the lowest XPS Ce/Al ratio in the H_2-reduced state and therefore the lower surface exposition. The formation of this strong Ce-alumina interaction in this sample probably leads to a poor Pt–Ce interaction. This poor Pt–Ce interaction could be the cause of Pt sintering observed in this sample after reduction. As consequence of that, the availability of Pt in the catalysts was not high enough to modify the catalytic behavior of NiACe catalyst. In addition, XRD patterns of the used Pt05NiACe sample showed a higher intensity of CeO_2 diffraction lines with respect to the XRD of the fresh reduced sample. The growth of the CeO_2 crystals during the reaction was not seen for the other catalysts and it might be also a reason for the poor stability of the sample: a lower Pt–Ce and Ni–Ce interactions would make more difficult the gasification of carbon performed by CeO_2 species, because it takes place in the Ce-metal interfaces [63].

For Pt contents $\geq$1 % in the catalysts, a better contact between Pt and Ce species is achieved. This higher Pt–Ce interaction facilitates the dispersion of small particles of Pt and thereby improves the reducibility of both Ce and Ni components at low temperatures. In this type of catalysts, the cooperative effect between Pt^0, Ni^0 and reduced Ce phases leads to an improvement in the stability of the catalyst. In other words: Ni provides activity in C–C bond breakage; Pt particles enhance the hydrogenation of coke precursors (C_xH_y) formed in the reaction, and Ce increases the availability of oxygen at the surface and thereby further enhances the gasification of carbon precursors.

5 Conclusions

Pt particles supported on Ni–Al–Ce systems have been observed to interact with the species existing at the surface of the catalysts; i.e. CeO_2, NiO, and, in particular, surface $NiAl_xO_y$. XPS showed that this interaction is not at electronic level (although the existence of partial electronic interaction at interface level between Pt and Ni particles could not be discarded) or by formation of alloys, but

mostly an enhancement in the reducibility of Ni and Ce species. As a consequence of the higher reducibility of $NiAl_xO_y$ surface species, catalysts containing Pt and Ce showed a higher overall metal surface exposition. Loadings of Pt $\geq$1.0 wt% provided a higher stability to the Ni/CeO_2–Al_2O_3 systems in ethanol steam reforming, in terms of lower carbon deposition and a constant production of CO_2 and H_2, with minor amounts of CH_4 and CO. The stabilization effect of Pt species was attributed to the ability of platinum to hydrogenate coke precursors, which are mostly formed on Ni particles. CeO_2 species were found to play an important role in dispersing Ni and Pt phases. In particular, the Pt–Ce interaction seems to be a key factor the dispersion and stabilization of Pt particles and therefore for the availability of Pt to modify the catalytic behavior of Ni supported species. To sum up, the most promising results in ethanol steam reforming were obtained for the Ni/CeO_2–Al_2O_3 catalyst with a content in Pt higher than 1.0 wt%. Lower loadings have proved to be insufficient to inhibit the production of C_2H_4 and carbon deposits.

Acknowledgments This research was supported by the Ministry of Science and Innovation (Spain) and the Autonomous Government of Madrid, Madrid (Spain) under grants ENE2010-21198-C04-01 and S2009ENE-1743, respectively.

References

1. Fatsikostas AN, Kondarides DI, Verykios XE (2002) Catal Today 75:145
2. Freni S, Cavallaro S, Mondello N, Spadaro L, Frusteri F (2002) J Power Sources 108:53
3. Haga F, Nakajima T, Miya H, Mishima S (1997) Catal Lett 48:223
4. Llorca J, Homs N, Sales J, de la Piscina PR (2002) J Catal 209:306
5. Fierro V, Klouz V, Akdim O, Mirodatos C (2002) Catal Today 75:141
6. Marino F, Boveri M, Baronetti G, Laborde M (2001) Int J Hydrogen Energy 26:665
7. Liguras DK, Kondarides DI, Verykios XE (2003) Appl Catal B 43:345
8. Fierro V, Akdim O, Provendier H, Mirodatos C (2005) J Power Sources 145:659
9. Breen JP, Burch R, Coleman HM (2002) Appl Catal B 39:65
10. Fatsikostas AN, Verykios XE (2004) J Catal 225:439
11. Zhang JC, Wang YH, Ma RY, Wu DY (2003) Appl Catal A Gen 243:251
12. Choudhary VR, Prabhakar B, Rajput AM (1995) J Catal 157:752
13. Parizotto NV, Rocha KO, Damyanova S, Passos FB, Zanchet D, Marques CMP, Bueno JMC (2007) App CatAL A Gen 330:12
14. Kugai J, Velu S, Song CS (2005) Catal Lett 101:255
15. Profeti LPR, Ticianelli EA, Assaf EM (2009) Int J Hydrogen Energy 34:5049
16. Sanchez–Sanchez MC, Navarro RM, Kondarides DI, Verykios XE, Fierro JLG (2010) J Phys Chem A 113:3873
17. Srinivas CVV, Satyanarayana CVV, Potdar HS, Ratnasamy P (2003) Appl Catal A Gen 24:323
18. Fatsikostas AN, Kondarides DI, Verykios XE (2001) Chem Commun 9:851
19. Srisiriwat N, Therdthianwong S, Therdthianwong A (2009) Int J Hydrogen Energy 34:2224
20. Zhang B, Tang X, Li Y, Cai W, Xu Y, Shen W (2006) Catal Commun 7:367
21. Alvarez-Galvan MC, Navarro RM, Rosa F, Briceno Y, Ridao MA, Fierro JLG (2008) Fuel 87:2502
22. Diagne C, Idriss H, Pearson K, Gomez-Garcıa MA, Kiennemann A (2004) C R Chim 7:617
23. Bunluesin T, Gorte RJ, Graham GW (1998) Appl Catal B Environ 15:107
24. Damyanova S, Perez CA, Schmal M, Bueno JMC (2003) Appl Catal A Gen 234:271
25. Trovarelli A (1996) Catal Rev Sci Eng 38:439
26. Zielinski J (1982) J Catal 76:157
27. Rynkowski JM, Paryjczak T, Lenik M (1993) Appl Catal A Gen 106:73
28. Ichikuni N, Murata D, Shimazu S, Uematsu T (2000) Catal Lett 69:33
29. Richardson JT, Twigg MV (1998) Appl Catal A Gen 167:57
30. Wang Y, Zhu A, Zhang Y, Au CT, Yang X, Shi C (2008) Appl Catal B Environ 81:141
31. Sanchez–Sanchez MC (2008) PhD Thesis, Universidad Autonoma de Madrid
32. Irusta S, Cornaglia LM, Lombardo EA (2004) Mater Chem Phys 86:440
33. Sheng PY, Bowmaker GA, Idriss H (2004) Appl Catal A Gen 261:171
34. Shyu JZ, Weber WH, Gandhi HS (1988) J Phys Chem 92:4964
35. Rynkowski JM, Paryjczak T, Lenik M, Farbotko M, Goralski J (1995) J Chem Soc, Faraday Trans 91:3481
36. Yao CH, Yao YF (1984) J Catal 86:254
37. Serre C, Garin F, Belot G, Maire G (1993) J Catal 141:1
38. Devred F, Gieske AH, Adkins N, Dahlborg U, Bao CM, Calvo-Dahlborg M, Bakker JW, Nieuwenhuys BE (2009) Appl Catal A Gen 356:154
39. Damyanova S, Perez CA, Schmal M, Bueno JMC (2002) Appl Catal A Gen 234:271
40. Corro G, Fierro JLG, Odillon VC (2003) Catal Commun 4:371
41. Ivanova AS, Slavinskaya SM, Gulyaev RV, Zaikovskii VI, Stonkus OA, Danilova IG, Plyasova LM, Polukhina IA, Boronin AI (2010) Appl Catal B Environ 97:57
42. Huizinga T, Vangrondelle J, Prins R (1984) Appl Catal 10:199
43. Salagre P, Fierro JLG, Medina F, Sueiras JE (1996) J Mol Catal A: Chem 106:125
44. NIST (2002) X-ray Photoelectron Spectroscopy Database: Version 3.4. National Institute of Standards and Technology, Gaithersburg. http://srdata.nist.gov/xp
45. Fujimori A (1985) J Magn Magn Mater 47:243
46. Wagner CD, Davis LE, Zeller MV, Taylor JA, Raymond RH, Gale LH (1981) Surf Interface Anal 3:211
47. Burroughs P, Hamnet A, Orchard AF, Thornton G (1976) J Chem Soc, Dalton Trans 17:1686
48. Paparazzo E (2011) Mater Res Bull 46:323
49. Wang SW, Lu GQ (1998) Appl Catal B Environ 19:267
50. Perrichon V, Retailleau L, Bazin P, Daturi M, Lavalley JC (2004) Appl Catal A Gen 260:1
51. Sánchez-Sánchez MC, Navarro RM, Fierro JLG (2007) Int J of Hydrogen Energy 32:1462
52. Huang YJ, Schwarz JA, Diehl JR, Baltrus JP (1988) Appl Catal 37:229
53. Di Cosimo JI, Diez VK, Xu M, Iglesia E, Apesteguia CR (1998) J Catal 178:499
54. Bartholomew CH (2001) Appl Catal A Gen 212:17
55. Wang SB, Lu GQ (1998) Energy Fuels 12:248
56. Kroll VCH, Swaan HM, Lacombe S, Mirodatos C (1996) J Catal 164:387

57. Luo JZ, Yu ZL, Ng CF, Au CT (2000) J Catal 194:198
58. Tsipouriari VA, Verykios XE (1998) J Catal 179:292
59. Seok SH, Han SH, Lee JS (2001) Appl Catal A Gen 215:31
60. Levy RB, Boudart M (1974) J Catal 32:304
61. Zheng W, Zhang J, Ge Q, Xu H, Li W (2008) Appl Catal B Environ 80:98
62. Fathi M, Bjorgum E, Viig T, Rokstad OA (2000) Catal Today 63:489
63. Bengaard RHS, Nrskov JK, Sehested J, Clausen BS, Nielsen LP, Molenbroek AM, Rostrup-Nielsen JR (2002) J Catal 209: 365